Biogeosciences, 21, 3271–3288, 2024
https://doi.org/10.5194/bg-21-3271-2024
© Author(s) 2024. This work is distributed under
the Creative Commons Attribution 4.0 License.

Biogeosciences Open Access EGU

Composite calcite and opal test in Foraminifera (Rhizaria)

Julien Richirt[1], Satoshi Okada[1], Yoshiyuki Ishitani[1], Katsuyuki Uematsu[2], Akihiro Tame[2], Kaya Oda[1], Noriyuki Isobe[3], Toyoho Ishimura[4], Masashi Tsuchiya[5], and Hidetaka Nomaki[1]

[1]SUGAR, X-star, Japan Agency for Marine-Earth Science and Technology (JAMSTEC), 2-15 Natsushima-cho, Yokosuka, Kanagawa, 237-0061, Japan
[2]Marine Works Japan Ltd., 3-54-1 Oppamahigashi-cho, Yokosuka, Kanagawa, 237-0063, Japan
[3]Research Institute for Marine Resources Utilization (MRU), Japan Agency for Marine-Earth Science and Technology (JAMSTEC), Yokosuka, Kanagawa, 237-0061, Japan
[4]Graduate School of Human and Environmental Studies, Kyoto University, Yoshidanihonmatsu, Sakyō-ku, Kyoto, 606-8501, Japan
[5]Research Institute for Global Change (RIGC), Japan Agency for Marine-Earth Science and Technology (JAMSTEC), Yokosuka, Kanagawa, 237-0061, Japan

Correspondence: Julien Richirt (richirt.julien@gmail.com)

Received: 10 January 2024 – Discussion started: 16 January 2024
Revised: 26 May 2024 – Accepted: 4 June 2024 – Published: 19 July 2024

Abstract. Foraminifera are unicellular eukaryotes known to have a shell, called a test, generally made of secreted calcite ($CaCO_3$). For the first time, we report a foraminifera with a composite calcite–opal test in the cosmopolitan and well-studied benthic species *Bolivina spissa* (Rotaliida), sampled from Sagami Bay in Japan at 1410 m depth. Based on comprehensive investigations including scanning electron microscopy (SEM) coupled with energy-dispersive X-ray spectroscopy (EDS) and Fourier-transform infrared (FTIR) spectroscopy, we inspect the morphology and composition of the novel opaline layer coating the inside part of the calcitic test. Using scanning transmission electron microscopy (STEM) and EDS analyses, we detected probable silica deposition vesicles (SDVs), organelles involved in opal precipitation in other silicifying organisms, confirming that the foraminifera itself secretes the opal layer. The layer was systematically found in all studied individuals and had no apparent substructure. Its thickness showed a growth pattern analogous to the calcitic shell of *B. spissa*, being the thickest in the oldest chamber (proloculus) and becoming thinner toward the younger chambers (apertural side). Its absence in the youngest chambers indicates that silicification occurs subsequent to calcification, probably discontinuously. We further discuss the potential function(s) of this composite test and propose that the opal layer may serve as a protective barrier against predators using either mechanical drilling or chemical etching of the calcitic test. Isotopic composition measurements performed separately on the proloculus part and the apertural side of *B. spissa* suggest that the presence of an opal layer may alter the calcitic isotopic signal and impact palaeoenvironmental proxies using foraminiferal test composition. If silicification in Foraminifera were found to be more widespread than previously thought, it could possibly have important implications for foraminiferal evolution, palaeoceanographic reconstructions, and the silica cycle at global scale.

1 Introduction

Silicon (Si) is the second most abundant element (27.2 wt %) in the Earth crust after oxygen (Greenwood and Earnshaw, 1997). In nature, Si occurs generally in the form of silicate minerals (e.g. quartz, aluminosilicates). Its soluble form, orthosilicic acid $Si(OH)_4$, is biologically available, and biogenic silica, also referred to as biogenic opal (amorphous hydrated silica, $SiO_2 \cdot nH_2O$), is the second most abundant mineral type formed by organisms after carbonate minerals. A wide range of marine organisms such as sponges and protists, including diatoms, radiolarians, and silicoflagellates (Dictyochales), are able to take up $Si(OH)_4$ from surrounding water and use Si to build their shells or skeletons (Brümmer, 2003;

Ehrlich et al., 2016). Silicified protistan shells serve various and not mutually exclusive functions, such as defence against grazers, buoyancy, light modulation, catalysis of carbon assimilation, maintenance of shape and orientation, or defence against viruses (Knoll and Kotrc, 2015).

Foraminifera (Rhizaria), belonging to the SAR group (i.e. Stramenopiles, Alveolata, and Rhizaria; Burki et al., 2020), are one of the most widespread unicellular eukaryotes inhabiting both benthic and pelagic realms. They are characterised by the presence of a shell, also called a "test", which can be organic or agglutinated (typically attaching sediment particles) or consist of precipitated minerals, most commonly calcium carbonate ($CaCO_3$; Sen Gupta, 2003). Having a high diversity with $\sim$ 4000 recent living hard-shelled species able to fossilise (Murray, 2007), they show a profuse fossil record starting in the Cambrian (Culver, 1991). Consequently, the group is intensively employed for palaeoceanographic studies and palaeoenvironmental reconstructions (e.g. Murray, 2006; Jones, 2013), and geochemical measurements of their tests have been extensively used to gain most of our knowledge on the past ocean responses to climate change (e.g. Katz et al., 2010). Additionally, Foraminifera play an important role in the global carbon cycle through carbonate production (Langer, 2008) and remineralisation, especially in poorly oxygenated environments (Piña-Ochoa et al., 2010; Cesbron et al., 2016). Although the exact calcification process is still up for debate (de Nooijer et al., 2014; Toyofuku et al., 2017; Nagai et al., 2018; Ujiié et al., 2023), different foraminiferal suborders are known to exhibit different test structure organisations (Hansen, 2003) and geochemical compositions (de Nooijer et al., 2023).

While silica precipitation occurs frequently in most of lineages of the SAR group (Marron et al., 2016), it has only very rarely been described in Foraminifera. The first report was made by Henry Bowman Brady in the late 19th century, who wrote that the tests of some benthic foraminifera assigned to Miliolina from the abyssal North Pacific were not dissolved by acid and that their usual calcareous shell was totally or partially replaced by a thin siliceous external coating, which exhibited a perfectly homogeneous texture (Brady, 1884, p. xvii). However, no supplementary information about this observation is available and these specimens might have been agglutinating foraminifera with a very smooth test. Almost 1 century later, Echols (1971) reported rare individuals of "*Miliolinella*" sp. presenting a wall that was insoluble in dilute hydrochloric acid, lacking apparent agglutinated particles, and possibly composed of opaline silica, in sediment sampled at various depths (990–4640 m water depth) in the Scotia Sea, the Southern Ocean. A benthic foraminiferal species sampled in the Indian Ocean at depths ranging from 5266–5420 m was also described as having an opaline shell, as it was insoluble in hydrochloric acid (*Miliammellus legis*, Saidova and Burmistrova, 1978). This species, being the only representative of the newly established genus *Miliammellus*, was placed into the order Miliolida because of its general morphology (Burmistrova, 1978). However, Lipps already argued in 1973 that insolubility in acids is not a conclusive result, because an organic cement would hold the test together, such as in specimens assigned to Rzehakinidae (Lipps, 1973), introducing foraminifera that have a "siliceous or agglutinated" wall that disaggregate in hydrogen peroxide but resist acid dissolution. Additionally, in the case of fossil species that do not disaggregate in hydrogen peroxide, taphonomic processes might have stabilised the organic matter cement, making this test inconclusive for fossilised specimens. Resig et al. (1980) described a species sampled from the Pacific Ocean at $\sim$ 4400 m depth that presented an imperforate test uniquely constituted of silica (*Silicoloculina profunda*; Resig et al., 1980) and created a new suborder (Silicoloculinina) based on the wall construction type (imperforate test made of secreted opaline silica). The authors imaged the fine structures of the test and investigated its composition, validating its opaline silica nature and concluding that the test was secreted by the foraminifera. The remarkable similarity regarding the descriptions given in Burmistrova (1978) and Resig et al. (1980) led to the conclusion that they certainly described the same species, making *Silicoloculina profunda* a junior synonym of *Miliammellus legis* (as referenced in the WoRMS database). The presence of silicate grains within the calcitic test was reported in *Melonis barleeanus* (Rotaliida), but these grains were inferred to be of sedimentary origin (Borrelli et al., 2018). While biosilicification has commonly been reported in other rhizarian groups such as radiolarians and cercozoans (Marron et al., 2016; Hendry et al., 2018), only scarce observations of foraminifera with a siliceous test have been reported and their silica mineralisation process is totally unknown. To date, *M. legis* (Miliolida) is the only species reported to have a secreted siliceous test for this group.

Here we report the systematic presence of an opaline layer in the test in the cosmopolitan benthic species *Bolivina spissa* (Rotaliida) sampled at 1410 m depth in Sagami Bay (Japan). The composite test is composed of two different materials: an external calcitic test, typical of hyaline and porcelaneous foraminifera, and an internal layer composed of biogenic silica (opal) coating the inside part of the calcitic test. Different observational and measurement methods were used to describe the composition, morphology, and presumed precipitation mechanism of this opal layer, including scanning electron microscopy (SEM), transmission electron microscopy (TEM), energy-dispersive X-ray spectroscopy (EDS), and Fourier-transform infrared (FTIR) spectroscopy. Based on these comprehensive observations, we discuss the potential function(s) of this composite test, its potential impact on palaeoenvironmental reconstructions using foraminifera test composition, and its possible importance for biogeochemical-cycle understanding.

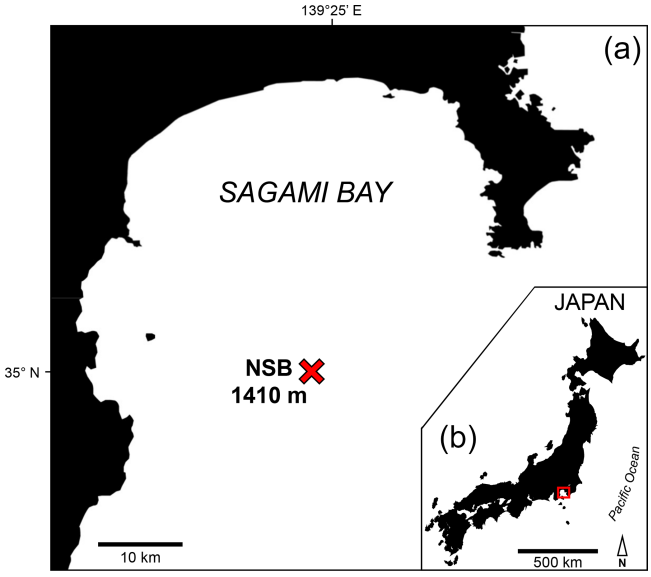

Figure 1. Map of Japan **(b)** indicating the localisation of Sagami Bay **(a)**. The NSB sampling site (red cross) and the sampling depth are indicated.

2 Material and methods

2.1 Sampling sites

Sediment cores were collected using the research deep submergence vehicle (DSV) *Shinkai 6500* on board R/V *Yokosuka*, in the central part of Sagami Bay (NSB site; 35°00.3′ N, 139°22.7′ E) at 1410 m depth (Fig. 1), during three sampling campaigns in May 2022 and 2023 and October 2022 (Table 1).

Table 1 summarises the samples' origin and the type of analyses performed. *Bolivina spissa* specimens were isolated from different sediment depth intervals (topmost centimetre or down to 5 cm depth) under a stereomicroscope and were fixed using different techniques (cryo-fixed on board – Okada et al., 2024; frozen at −80 °C, glutaraldehyde fixed, or air-dried).

2.2 Cryo-SEM imaging and EDS mapping

After confirming that individuals were alive (based on the presence of sediment aggregation at the aperture and cytoplasm colouration), isolated specimens were processed following the protocol described in Okada et al. (2024). Briefly, specimens were embedded in a sucrose-based or glycerol-based aqueous glue, cryo-fixed (in liquid nitrogen-cooled isopentane), and stored at ca. −170 °C. Cross-sections of the specimens were exposed using a diamond knife in a cryo-ultramicrotome, aiming for a clean cut to eliminate topographic variations in the sample surface. Scanning electron microscopy (SEM) observations were performed on a Helios G4 UX (Thermo Fisher Scientific) equipped with a gallium focused ion beam (FIB) gun, an energy-dispersive X-ray spectroscopy (EDS) detector (Octane Elite Super C5, AMETEK), and a cryogenic stage with a preparation chamber (PP3010T, Quorum). After sublimation of overlying ice crystals (∼ 5 min at ∼ −80 °C), several SEM images in backscattered electron mode were acquired and aggregated to obtain a high-resolution SEM image for each individual ($n = 7$). The elemental composition was then mapped by EDS analysis without conductive coating of the sample to avoid the possible overlap of EDS peaks from the coating metals.

After spectral treatment to deconvolve signal from noise (correction for the bremsstrahlung effect, Method S1 in the Supplement), the colocalisation of SEM images and EDS elemental maps was performed manually using calcium distribution maps (Ca EDS), the main component of calcitic tests (SEM images). Scaling and/or rotation of EDS maps was performed when necessary, but deformation (i.e. warping) was never applied. Finally, to obtain an Si map of non-sedimentary origin, the aluminium (Al) signal was subtracted from the silicon (Si) signal to remove aluminosilicate particles (typically clay minerals, the major constituent of sediment at the sampling site) from EDS maps. Additional individuals belonging to the genera *Uvigerina*, *Chilostomella*, and *Globobulimina* and isolated from the same sample site were also studied with a similar procedure.

Finally, the thickness of the Si layer was measured in each separate chamber (numbered from the proloculus toward the apertural side) on all available *B. spissa* specimens.

Image treatments and measurements were performed using Fiji software (Schindelin et al., 2012).

2.3 Low-vacuum SEM imaging

To expose the Si layer below the calcitic test, isolated and air-dried individuals ($n = 15$) were subsequently immersed in 0.5 M ethylenediaminetetraacetic acid disodium salt solution (EDTA, 03690 – Sigma-Aldrich) for 48 h and then rinsed with distilled water before observation. Subsequently, specimens were put on an aluminium stub on carbon tape prior to observation with a benchtop SEM instrument (JEOL JCM-6000Plus) in low-vacuum mode, without coating, at 15 kV acceleration voltage and using backscattered electron mode. Optical images using a camera mounted on a stereomicroscope were obtained both before and after the decalcification step. Additional individuals belonging to the genus *Bulimina* and isolated from the same sample site were also imaged with the same procedure.

2.4 TEM imaging and EDS measurements

To search for potential organelles involved in biosilicification, we observed the contents of the cytoplasm using transmission electron microscopy (TEM) and performed high-angle annular dark-field scanning transmission electron microscopy (HAADF-STEM) coupled with EDS analyses. Di-

Table 1. Sampling period, sediment interval, type of analysis, fixation type and timing and number of specimens analysed in this study.

Sampling period	Sediment interval	Type of analysis	Fixation type	Fixation timing	Number of specimens analysed
May 2022	0–1 cm	Cryo-SEM and EDS	Cryo-fixed	Isolated ∼ 1.5 months after sampling from a bucket of sediment stored in the lab at 4 °C	1
October 2022	0–1 cm	Cryo-SEM and EDS	Cryo-fixed	Cryo-fixed directly on board after sampling	6
May 2022	0–1 cm and 1–5 cm	Environmental SEM	Frozen at −80 °C	Sample frozen at −80 °C directly on board after sampling	15
May 2022	Every centimetre from 0–1 to 3–4 cm	TEM and EDS	Glutaraldehyde 4 %	Fixed directly on board after sampling	8
May 2023	0–2 cm	FTIR spectroscopy	Air-dried	Isolated ∼ 3 months after sampling from a bucket of sediment stored in the lab at 4 °C	3
October 2022	0–5 cm	Isotopic composition of calcite	Air-dried	Isolated ∼ 2 months after sampling from a bucket of sediment stored in the lab at 4 °C	17

rectly on board, living specimens ($n = 8$) were isolated from different sediment layers of 1 cm thickness (0–1 to 4–5 cm depth) and were fixed with glutaraldehyde. Specimens were then embedded in 1 % aqueous agarose and cut into ∼ 1 mm cubes. Samples were decalcified with 0.2 % ethylene glycol tetraacetic acid (EGTA) in 0.81 mol L^{-1} aqueous sucrose solution (pH 7.0) for several days, rinsed with filtered seawater, and postfixed with 2 % osmium tetroxide in filtered seawater for 2 h at 4 °C. Samples were rinsed with an 8 % aqueous sucrose solution and stained with 1 % aqueous uranyl acetate for 2 h at room temperature. Stained samples were rinsed with Milli-Q water, dehydrated in a graded ethanol series, and embedded in epoxy resin. Blocs were further sectioned into ultra-thin sections (60 nm thick) which were then placed on a formvar-supported copper grid mesh and subsequently stained with 2 % aqueous uranyl acetate and lead stain solution (0.3 % lead nitrate and 0.3 % lead acetate, Sigma-Aldrich). TEM observations were performed with a bottom-mounted 2k × 2k Eagle charge-coupled device camera (Tecnai G2 20, Thermo Fisher Scientific). Elemental compositions were obtained by EDS analyses performed using an EDAX Genesis system under scanning transmission electron microscopy (STEM) mode operating at an acceleration voltage of 120 and 200 kV, respectively.

2.5 FTIR spectroscopy

The topmost 2 cm of sediment from the NSB station was sieved through a 63 µm mesh sieve, and *B. spissa* specimens were isolated from the residue. Only specimens showing a completely empty shell and having a translucid appearance were selected to avoid the presence of remaining cytoplasm in the test. To remove the calcitic layer and expose the underlying Si layer of the test, empty tests were then immersed in 0.5 M of EDTA (03690, Sigma-Aldrich) for 24 h, rinsed with Milli-Q water, placed on a calcium fluoride (CaF_2) plate, and dried in a vacuum chamber prior to measurement. Dried samples were measured using a microscope Fourier-transform infrared spectrometer (FT/IR-6200 with IRT-7000, Jasco Inc.) with an aperture size of 15 µm × 15 µm. Transmission IR signals were background-corrected to determine the infrared spectra between 4000–750 cm^{-1} in the spectral region for a total of three specimens. CaF_2 absorbs below 1000 cm^{-1}; therefore no band assignments were made in this region (Mayerhöfer et al., 2020).

2.6 Isotopic analyses

In total, 17 specimens of *B. spissa* with transparent shells were isolated from NSB site sediment (Fig. S1 in the Supplement), cleaned with Milli-Q water, and carefully examined under a stereomicroscope to confirm the absence of authigenic particles (Ishimura et al., 2012). Individuals were micro-dissected in two parts using a scalpel, aiming to separate the oldest part (proloculus side) from the newest part of the test (apertural side). Because it was challenging to dissect only the proloculus from the other chambers on the apertural side, a few chambers were still attached to the proloculus prior to analysis (6 microspherical and 11 macrospherical individuals, Fig. S1). Stable carbon and oxygen isotopic compositions ($\delta^{13}C$ and $\delta^{18}O$, respectively) of dissected parts were determined using a high-precision microscale carbonate isotopic analytical system, MICAL3c (Ishimura et al., 2004, 2008). Samples were reacted with phosphoric acid (H_3PO_4) to decompose $CaCO_3$ and produce CO_2. Note that with the same method, Ishimura et al. (2012) reported that no CO_2 was evolved through the reaction between H_3PO_4 and organic materials at 25 °C over several days. After pu-

rification, CO_2 was introduced into an IsoPrime100 isotope ratio mass spectrometer (Isoprime Ltd., Cheadle Hulme, UK) equipped with a customised continuous-flow gas preparation system (MICAL3c) at Kyoto University. This system allows us to determine the $\delta^{13}C$ and $\delta^{18}O$ values of as little as 0.1 µg of $CaCO_3$ with an analytical precision of better than ± 0.10 ‰. The isotopic values were standardised to the Vienna Pee Dee Belemnite (VPDB) scale and expressed in δ notation. The mass of dissected samples was estimated from the volume of CO_2 gas produced during the reaction between $CaCO_3$ and H_3PO_4.

3 Results

3.1 Morphology of the Si coating the inside part of the calcitic test

Macrospherical (haploidic) and microspherical (diploidic) specimens were observed with a stereomicroscope (Fig. 2a and b) before being imaged in low-vacuum SEM settings (Fig. 2c and d). Specimens showed a costate proloculus, acute carinate edges, and sometimes a minute apical spike, typical of the morphospecies *Bolivina spissa*. The same specimens were then imaged with low-vacuum SEM settings (Fig. 2e and f) after the dissolution of their calcitic shell to expose the underlying Si layer. In all individuals, the final (newer) chambers were always missing and/or collapsed after decalcification, while the older chambers on the proloculus side remained well shaped (Fig. 2e and f).

Figure 3a shows the Si layer connections between consecutive chambers after the removal of the calcitic test by decalcification. Protruding funnel-like structures were visible at the pores' location after decalcification, coating the inner surface of the original pore's calcitic wall (Fig. 3b). These funnel-like structures were not made of Si but were probable remains of organic material, as cryo-SEM (Fig. 3c) and TEM observations (Figs. S2 and S3) show the Si internal coating terminates at the pore plate. The texture of the Si layer's surface always appeared smooth without visible substructures (excluding where pores priorly occurred), and the proloculus was nearly spherical (Fig. 3d). None of the individuals belonging to the other investigated genera (i.e. *Uvigerina*, *Chilostomella*, *Globobulimina*, and *Bulimina*) showed an Si layer.

Figure 4 illustrates the workflow used to obtain the Si distribution maps of non-sedimentary origin which were finally superimposed on the cryo-SEM images. The calcium distribution (Fig. 4a and b) followed the electron-dense-area SEM images (Fig. 4c and d) representing the calcitic test of individuals. Sedimentary aluminosilicates were removed by subtracting the aluminium signal from that of Si (Fig. 4e–j), and the resulting signal showed that the Si was localised on the inner wall of the calcite test (Fig. 4k–l). The Si lining of non-sedimentary origin was systematically found in all the seven specimens analysed (Table 1), and the Si signal was always stronger in the older chambers (proloculus side) than in the newer chambers (aperture side, Fig. 4i–l).

The Si layer was clearly identifiable on cryo-SEM images as a less electron-dense structure coating the internal part of the calcitic test (Fig. 5). The thickness of this Si layer was constant inside individual chambers for a given specimen. The decreasing Si signal from the proloculus to apertural side detected on EDS maps (Fig. 4i–l) was confirmed by cryo-SEM observations showing decreasing Si layer thickness toward younger chambers (Fig. 5). The Si layer was homogeneous without any visible layering even on the thickest sections and exhibited conchoidal fractures, which is typical of glassy materials (Fig. 5e). No other visible structures were observed between the Si layer structure and the calcitic shell, which were in direct contact. In very rare cases, we observed a gap between the two layers, such as in Fig. 5e, that we ascribe to preparation artefacts (i.e. the cutting step).

The thickness of the Si layer was equivalent considering each separate chamber and ranged from 1.65 to 0.05 µm measured in the proloculus part and in the last chamber of the individual where the Si layer was still visible, respectively (Table S1 in the Supplement). Data presented here must be considered carefully because a sub-perpendicular cracking orientation could introduce a bias into the actual thickness of the Si layer in each specimen. The Si layer was not visible in chambers younger than chamber 12 when the number of visible chambers was higher than 12 in five of the seven specimens (Table S1). However, the cryo-SEM image resolution might have not been sufficient to detect structures smaller than 0.05 µm, corresponding to about 4 pixels in the acquired images. Thickness data indicated that the decreasing trend in the Si layer thickness follows an inverse power law ($r^2 = 0.99$, Fig. 6).

3.2 Infrared spectral analyses

For all three *B. spissa* specimens and all chambers, FTIR spectra (Fig. 7) displayed a strong absorption band at $\sim 1070\,cm^{-1}$ with an associated shoulder at $\sim 1250\,cm^{-1}$ that is attributed to asymmetric Si–O–Si stretching vibrations (Socrates, 2004; Larkin, 2011). The broad bands at $3400\,cm^{-1}$ and at $\sim 1635\,cm^{-1}$ are ascribed to the O–H stretching of absorbed water (Socrates, 2004; Larkin, 2011), matching with opal. The IR spectra from the proloculus showed a broader band at $\sim 1070\,cm^{-1}$ with a shoulder at $\sim 1250\,cm^{-1}$, while a small peak from C–H stretching was observed at $\sim 2930\,cm^{-1}$ in spectra of the eighth chamber.

3.3 TEM imaging and STEM-EDS measurements

To investigate the putative organelles involved in silica deposition, ultra-thin sections of *B. spissa* individuals were imaged with TEM (Fig. 8a). From a total of eight individuals imaged, two showed structures filled with material show-

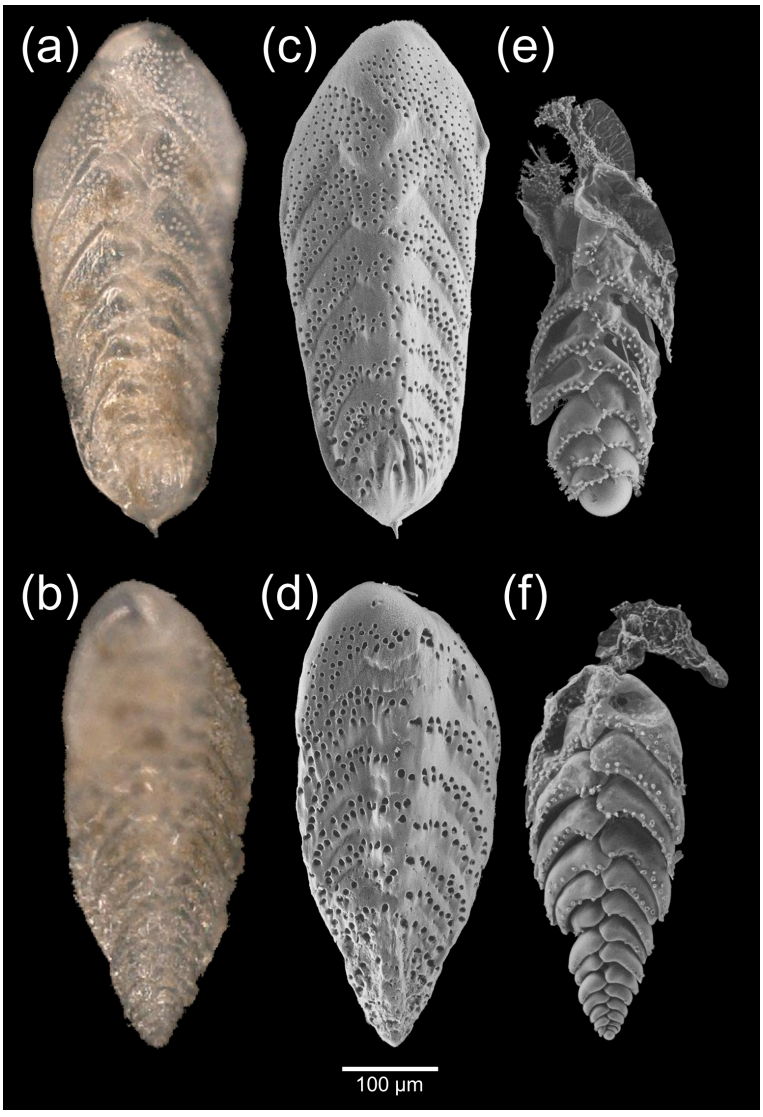

Figure 2. Macrospherical **(a, c, e)** and microspherical **(b, d, f)** *Bolivina spissa* specimens, imaged with a stereomicroscope **(a, b)** and low-vacuum SEM before **(c, d)** and after **(e, f)** decalcification to expose the Si layer below the calcitic shell.

ing the characteristic conchoidal fracture pattern of Si-based materials (Fig. 8b–g). This conchoidal fracture pattern when sectioned with a diamond knife was also clear on the Si layer coating the inside part of the calcitic shell, which was visible on all eight specimens (Fig. S2). Note that the appearance of these structures on TEM images is presumably denatured during sample preparation, such as previously reported for other silicifying organisms (Garrone et al., 1981).

STEM-EDS analyses indicated that the electron-dense material in these vesicles was mainly composed of Si and showed a similar spectrum to the Si layer coating the internal part of the calcitic test (Fig. S4). These organelles are remarkably similar to silica deposition vesicles (SDVs) described in other biosilicifying organisms (Anderson, 1994; Foissner et al., 2009). The elemental composition of the content of these SDV-like organelles was different from vesicles filled with sediment material where Si was mostly associated with Al (aluminosilicates, such as feldspars, which are abundantly found in the sediment, Fig. S4). The latter vesicles, filled with sediment and organic detritus, occur abundantly in the cytoplasm of *B. spissa* and represent food vacuoles (Goldstein and Corliss, 1994).

3.4 Isotopic analyses

The calcite mass of dissected samples ranged between 0.2 and 2.9 µg for the proloculus side and 1.1 and 13.6 µg for the apertural side (Table S2). The proloculus side of dissected samples exhibited low $\delta^{18}O$ values ranging from +0.13 ‰ to +3.09 ‰ compared with the aperture side, which ranged from +2.11 ‰ to +3.11 ‰. The $\delta^{18}O$ values of the aperture

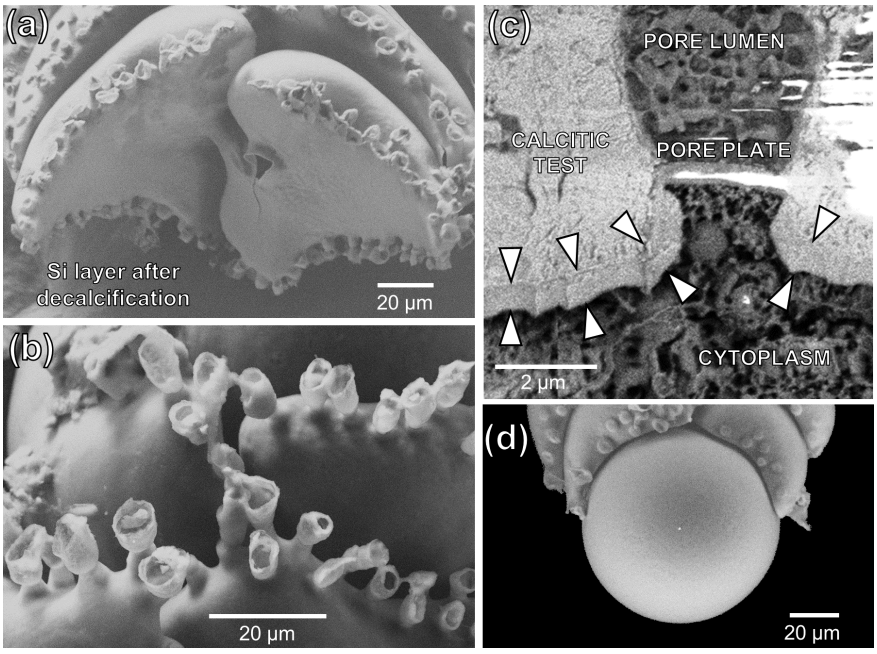

Figure 3. SEM images of the silicified structures of *B. spissa*. **(a)** Broken *B. spissa* after decalcification to expose the Si layer connections between successive chambers. **(b)** Magnification of the pore funnel-like structures of *B. spissa* exposed after decalcification. **(c)** Transversal section of a pore imaged with cryo-SEM on non-decalcified *B. spissa*. White arrows indicate the position of the Si layer. The white colour in the top right of the image and on the pore plate is due to overcharging. **(d)** Magnification of the proloculus of *B. spissa* exposed after decalcification.

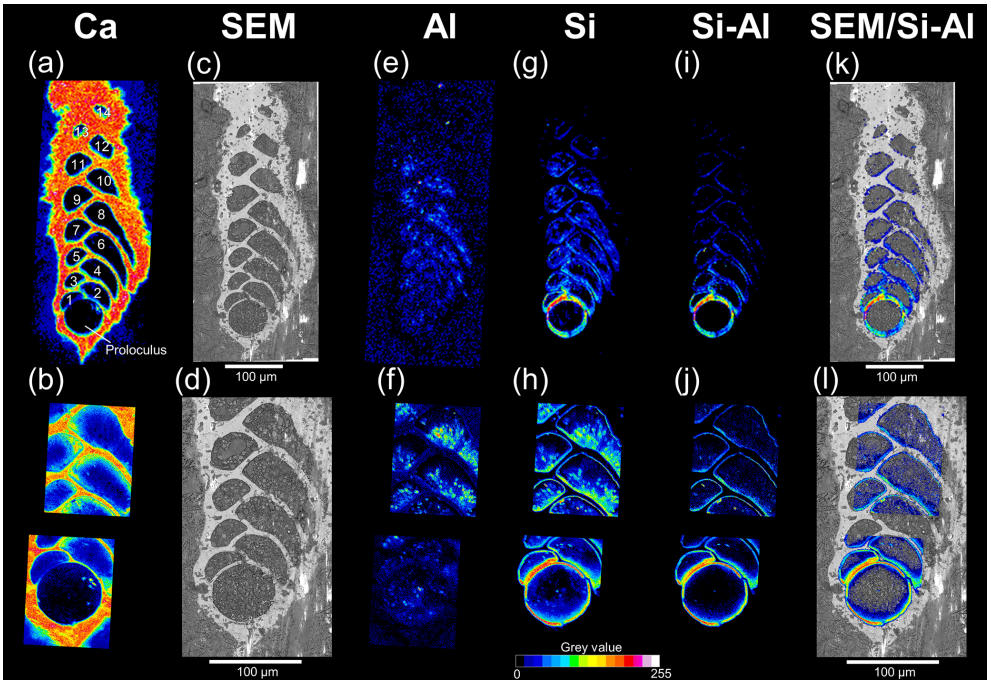

Figure 4. SEM imaging and EDS maps (16 colours, grey-value scale) of a representative cryo-fixed *B. spissa* **(a, c, e, g, i, k)** and magnification of areas of interest **(b, d, f, h, j, l)**. **(a, b)** EDS maps of Ca used to colocalise EDS elemental maps and SEM images. The proloculus is indicated, and chambers are numbered. **(c, d)** SEM images of a cryo-cracked specimen. **(e, f)** EDS maps of Al. **(g, h)** EDS maps of Si. **(i, j)** Resulting EDS maps from the subtraction of the Al signal from the Si signal (i.e. removing aluminosilicates). **(k, l)** Superimposition of Si map of non-sedimentary origin over SEM images.

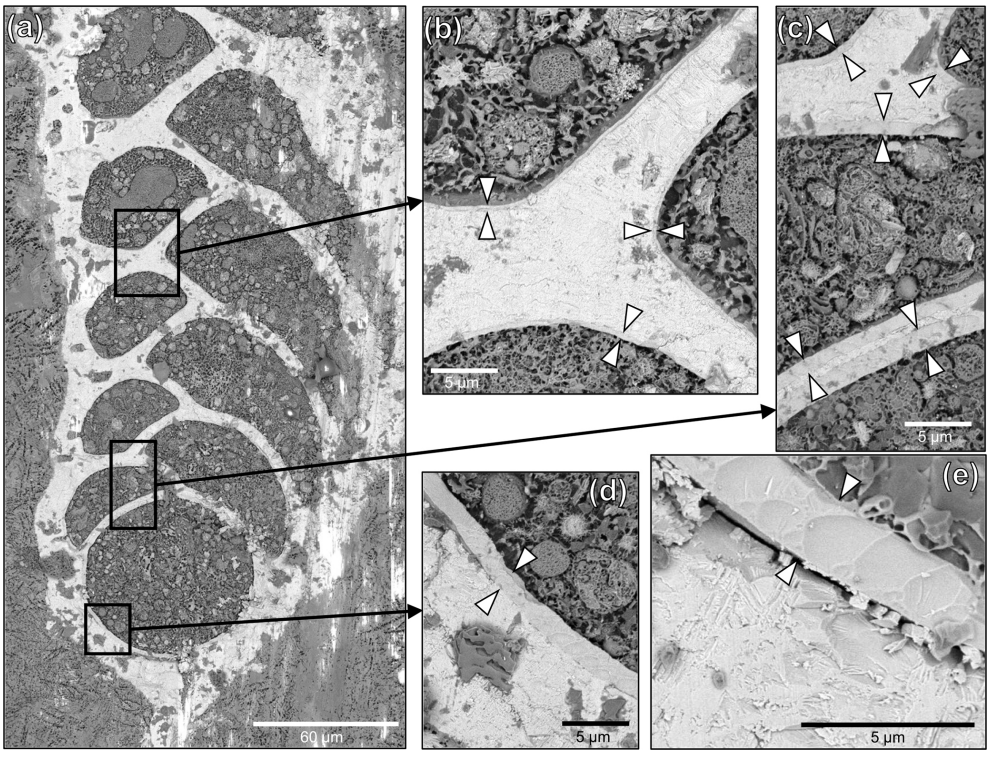

Figure 5. Cryo-SEM images of a representative cryo-cracked *B. spissa* specimen. **(a)** Overview of the specimen and **(b–e)** magnified regions of interest (black squares) to visualise the Si layer (indicated by white arrowheads) coating the inside part of the calcitic test. Note the decreasing thickness of the layer from the proloculus toward newer chambers. **(e)** Magnified cryo-SEM image of the Si layer in the proloculus showing the homogeneity of the structure. Note the conchoidal fracture pattern typical of glassy materials. The gap between the calcitic shell and the Si layer was very rarely observed and results from a preparation artefact.

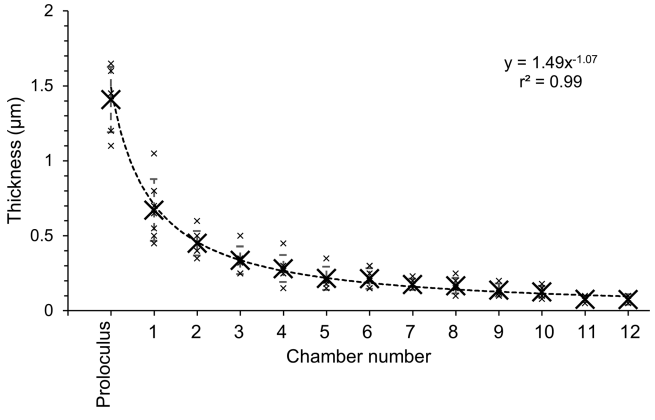

Figure 6. Plot representing the thickness of the Si layer as a function of the chamber number (numbered as indicated in Fig. 4a) measured on seven individuals. Measurements (small black crosses) were averaged by chamber (big black crosses), and the standard deviation is represented by error bars. The dashed black line is a power law trend line based on averaged values.

side were comparable to the isotopic equilibrium value of calcite at a depth of 1100 m in Sagami Bay (Ishimura et al., 2012). Specimens exhibiting low $\delta^{18}O$ values also showed low $\delta^{13}C$ values. This trend was observed for both microspherical and macrospherical individuals (Fig. S5). Lower $\delta^{18}O$ and $\delta^{13}C$ values were typically found in smaller (i.e. younger) specimens, which had a test length ranging from 200 to 400 µm (Fig. S6).

4 Discussion

4.1 Composite test made of calcite and opal

The Si layer, which was systematically observed in all studied *B. spissa*, is composed of biogenic opal (amorphous hydrated silica, $SiO_2 \cdot nH_2O$). This was firstly indicated by the cross-sections of the Si layer exposed by diamond knife cutting on cryo-SEM and TEM images, both showing a conchoidal fracture pattern (Figs. 5e and S2) that is typical of amorphous glass and well known for a variety of Si-based organisms (see review in Garrone et al., 1981). This was further confirmed by FTIR spectra obtained on decalcified empty tests (translucid, dead), which were in good agree-

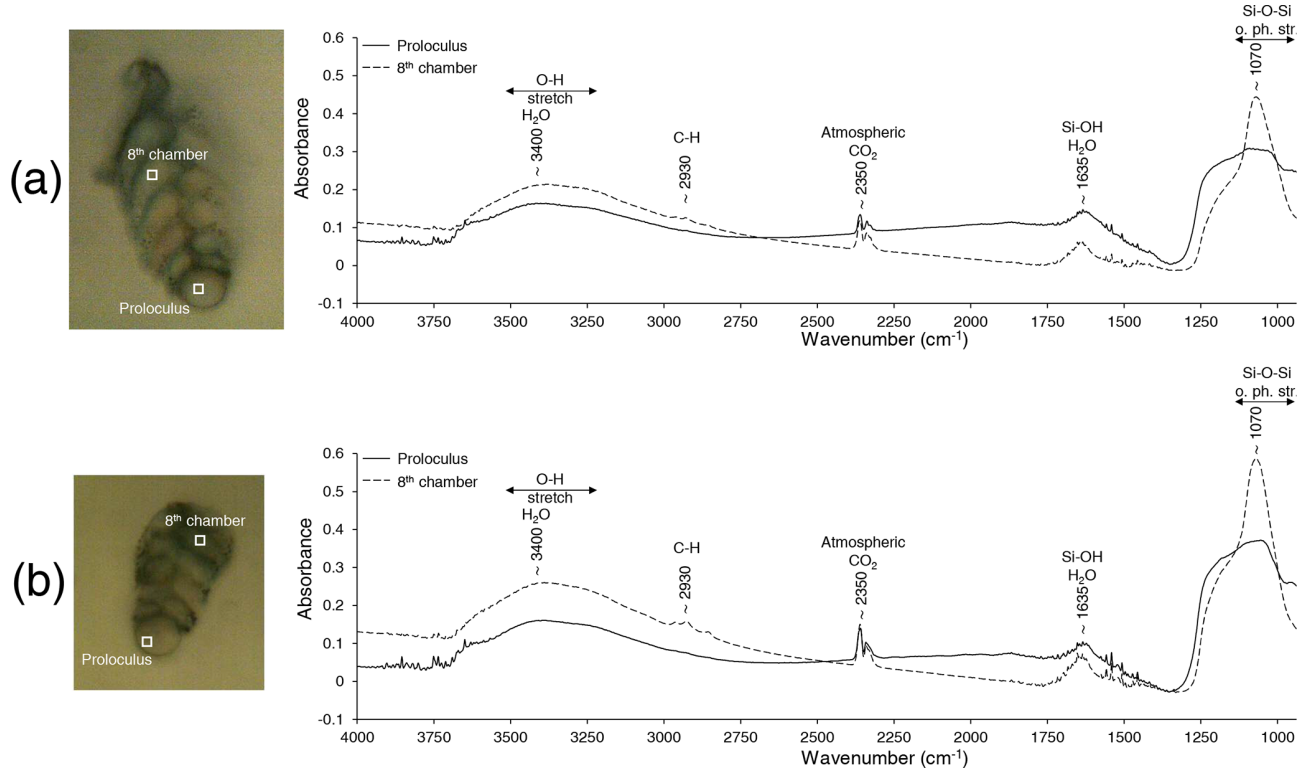

Figure 7. Representative FTIR spectra measured on the proloculus (solid line) and the eighth chamber (dotted line) for two decalcified specimens **(a, b)** of *B. spissa*. The term "o. ph. str." denotes out-of-phase stretching.

ment with spectra of reference opal (Lowenstam, 1971), diatom frustules (De Stefano et al., 2005), and diatomite (Reka et al., 2021) spectra. This is congruent with previous measurements on *Miliammellus legis* in Resig et al. (1980), for which the test material spectra also matched the opal reference of Lowenstam (1971).

The opal layer coating the inside part of the calcitic test of *B. spissa* appears to be homogeneous, without any visible substructures even in high-resolution SEM images. This is different from *M. legis*, for which the test, made entirely of opal, is formed by a median layer (18 µm thick) composed of fused tubular rods randomly arranged in a three-dimensional open mesh. This median layer is framed by an inner and an outer layer (1 µm thick each), both composed of tightly packed rod sheets parallel to the inner and outer surface, respectively, of the shell (see Plates 2 and 3 in Resig et al., 1980). These morphological and structural differences suggest different precipitation processes between the two genera, as is the case for the carbonate tests of Miliolida and Rotaliida, to which *Miliammellus* and *Bolivina*, respectively, belong (Parker, 2017; Dubicka, 2019).

In *B. spissa*, the opal layer thickness was constant within each chamber but was not equivalent between chambers in a given individual, always being the thickest in the proloculus and becoming thinner toward the newer chambers at the apertural side of the test. This decreasing trend in thickness is analogous to the calcitic tests in Foraminifera having a lamellar wall (such as *Bolivina*), which covers the entire test with new calcitic material (i.e. outer lamellae) when adding a new chamber and results in a decreasing thickness of the calcitic test from the proloculus toward the newest chamber (Hansen, 2003). The outer lamellae covering the entire test when adding a chamber progressively decrease in thickness, so the more layers that are added, the more difficult the outer lamellae become to trace (Bé and Lott, 1964). In some of our *B. spissa* specimens, we observed such a decreased outer lamellae thickness toward external calcite layers in cryo-SEM images. The opal layer thickness from the proloculus toward the apertural side of the test follows an inverse power law (Fig. 6), suggesting that it results from an ontogenetic effect. This decreasing thickness trend, similar in both calcite and opal, coupled to the observation of an opal coating in young specimens (i.e. with few chambers) indicates that the opal layer is not formed during a single event but during multiple discrete steps, comparable to the precipitation pattern for the calcitic test. However, even in the proloculus where its thickness was at a maximum, no layered substructures were visible in the opal layer (Figs. 3d and 5e).

After decalcification, the youngest chambers on the apertural side were always collapsed or absent (Fig. 2e and f) either because the opal layer was too thin to maintain its chamber-shaped structure or because of its absence in the

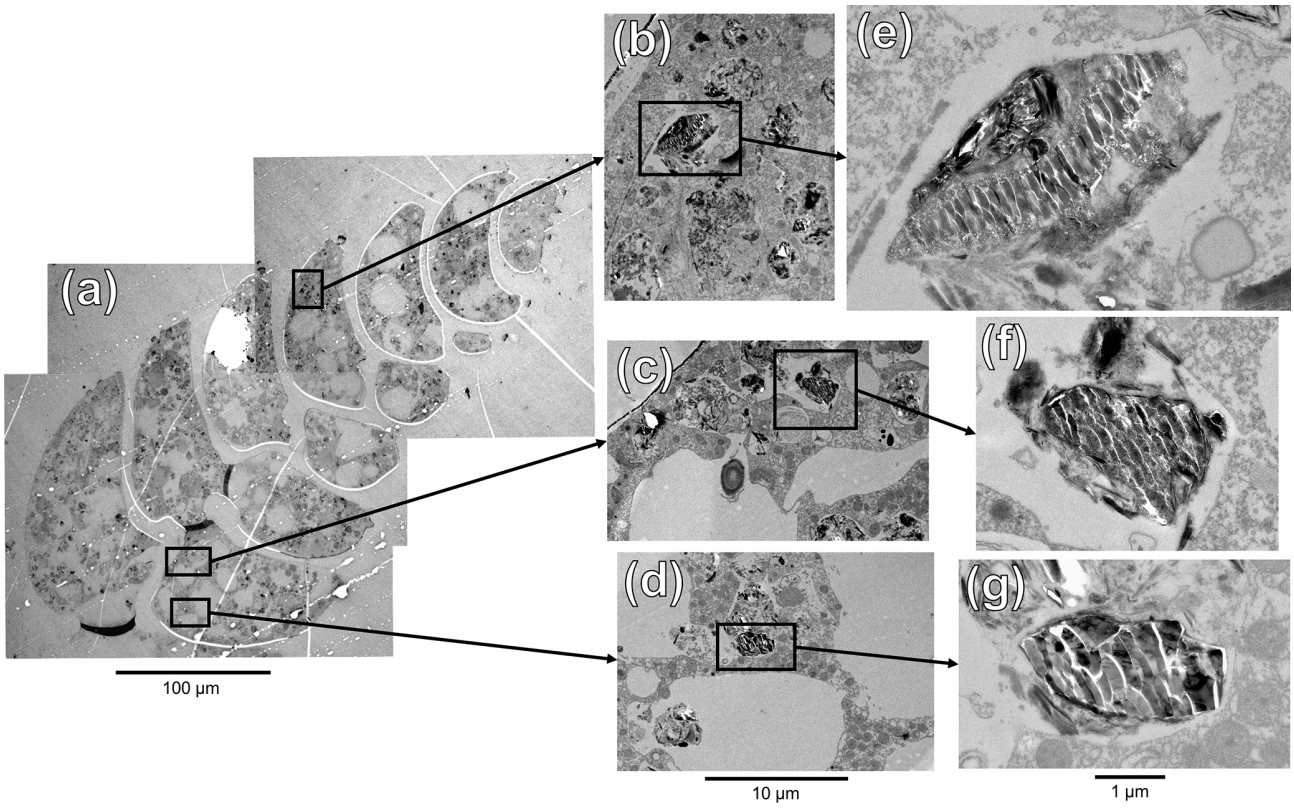

Figure 8. TEM images of an ultra-thin section of *B. spissa* specimen **(a)**. **(b–d)** Magnified regions of interest represented by black squares in **(a)**. **(e–g)** Further magnified areas of the black squares in **(b)**–**(d)**, respectively.

newest part of the test. This is corroborated by cryo-SEM and TEM image observations, where no opal layer was visible in the newest chamber(s) (Figs. 5a, 8a, and S7). The absence of an opal layer in the newest calcified chambers indicates that its formation must occur after the precipitation of the calcitic shell.

4.2 Is the opal layer precipitated by the foraminifera itself?

Several observations indicate that the opal layer is secreted by the foraminifera itself and is not due to specific environmental conditions or any other passive process(es):

1. The layer is systematically present in all *B. spissa* sampled during 2 consecutive years (May and October 2022 and May 2023), which were isolated from different depth intervals in the sediment and hence exposed to different environmental conditions (e.g. oxic/anoxic).

2. The layer only coats the inside part of the calcitic shell, suggesting that it results from a mechanism taking place inside the calcitic test (i.e. in the cell and not in the surrounding water).

3. The layer is observed in living specimens, demonstrating that the deposition process occurs while the individual is alive.

4. The layer is not observed in any other species found at the same site, such as individuals belonging to *Uvigerina*, *Chilostomella*, *Globobulimina*, or *Bulimina* genera, indicating that opal formation in *B. spissa* is not the result of a passive process.

5. The smooth and homogeneous appearance of the layer suggests that it results from a precipitation process and not an aggregation of particles of allochthonous origin (e.g. of sedimentary or biogenic origin, i.e. secreted by another organism and subsequently incorporated by the foraminifera).

6. The opal layer thickness follows an allometric relationship (i.e. inverse power law), from the proloculus (thick) to newer chambers (thin), commonly found in organisms' growth patterns and suggesting that the layer results from an ontogenetic process, analogously to the secreted calcitic test.

Supplementary TEM observations reveal peculiar organelles that occur in the cytoplasm and contain material exhibiting the typical conchoidal fracture pattern in TEM im-

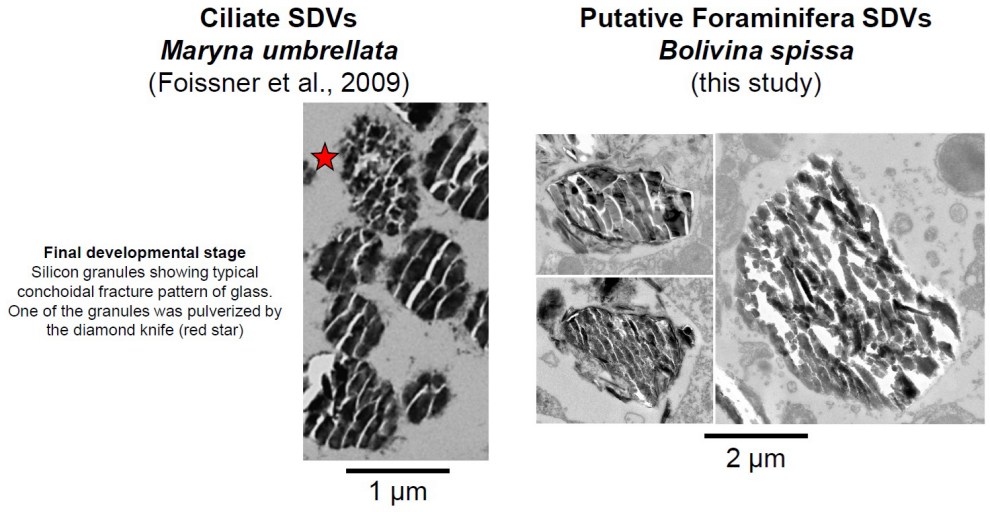

Figure 9. TEM images showing the final development stage of the Si granules in SDVs in the ciliate *Maryna umbrellata* (modified from Foissner et al., 2009) and organelles in *B. spissa* exhibiting similar appearance, hence representing putative SDVs. Note the scale difference, which is 2 times larger for *B. spissa* than for the ciliate.

ages and opal composition in EDS spectra (Figs. 8 and S4). These findings further corroborate the assertion that the foraminifera secretes the opal layer itself. These organelles are strikingly similar to silica deposition vesicles (SDVs), involved in the secretion of opal in frustules of diatoms (Drum and Pankratz, 1964) or the shell of other organisms in the SAR group (Anderson, 1994; Foissner et al., 2009; Fig. 9) to which Foraminifera belong. While *B. spissa* was shown to feed selectively on fresh phytodetritus transported from the surface ocean (e.g. diatoms; Nomaki et al., 2006), the appearance of these organelles greatly differs from typical diatom frustules ingested by foraminifera (e.g. see Fig. 9D in Jauffrais et al., 2018, and Fig. 4D in Goldstein and Corliss, 1994; Fig. S8) or sponge spicule (Garrone et al., 1981), indicating that they do not represent remains from these organisms. We consider these organelles to be SDVs (Figs. 8 and 9), which have never been reported before in Foraminifera (see review in LeKieffre et al., 2018). The observation of these SDV-like organelles in two out of eight individuals analysed in total supports the hypothesis that the opal deposition process takes place intermittently or that these organelles occur rather rarely in the cytoplasm of *B. spissa*. SDV-like organelles were observed in both younger and older chambers of the same specimen (Fig. 8), suggesting that opal layer deposition might occur simultaneously in different chambers and resulting in thicker layers in older chambers. These organelles were observed in individuals from a 1–2 cm depth interval in the sediment, where oxygen is absent (Glud et al., 2009), suggesting that opal precipitation may occur in anoxic settings, as has been shown for calcite precipitation (Nardelli et al., 2014; Orsi et al., 2020). Further analyses, such as a transcriptomic study targeting genes involved directly in silica precipitation or biosilicification, are necessary to conclusively determine the exact nature of these organelles.

The existence of a secreted opal layer coating the inside part of the calcitic test highlights a new biosilicification process in *B. spissa*, making this species the first Rotaliida able to secrete opal and the first Foraminifera able to precipitate both materials (i.e. calcite and opal) ever reported on in the literature.

The only other known biosilicifying foraminifera is *M. legis* (Miliolida; Burmistrova, 1978), which branches relatively far from *Bolivina* (Rotaliida) in phylogenetic trees based on 18S rRNA (e.g. Pawlowski et al., 2013) or multi-gene phylogenies (Groussin et al., 2011; Krabberød et al., 2017; Sierra et al., 2022; Fig. S9a). These phylogenetic relationships, in which Rotaliida and Miliolida are nested within naked foraminifera, suggest that biosilicification was acquired independently throughout their evolution history. Similarly, it has been previously suggested that different test organisations and/or compositions and calcification pathways likely emerged multiple times during foraminiferal evolution in different foraminiferal orders, especially between Rotaliida and Miliolida (Groussin et al., 2011; Pawlowski et al., 2013; Holzmann and Pawlowski, 2017; Sierra et al., 2022; de Nooijer et al., 2023). The distinct appearance and microstructure of the opaline shell found in *B. spissa* compared to *M. legis* support the idea that this trait emerged independently in both *Bolivina* and *Miliammellus*. However, we cannot exclude the hypothesis that biosilicification was inherited from a common ancestor (of rhizarians for instance) and that this trait was lost in most other foraminifera. Silicon transporter (*SIT*) genes putatively inherited from a common eukaryotic ancestor have previously been identified in other well-studied rotaliid Foraminifera

that are not known to exhibit any opaline silica structures (i.e. *Ammonia*, *Elphidium*, and *Rosalina*; Marron et al., 2016; Fig. S9b). This finding confirms that the presence of *SIT* genes does not necessarily imply the capacity to precipitate opaline silica and rather corroborates the common-ancestor hypothesis. To investigate the exact origin of biosilicification in Foraminifera from an evolutionary point of view, further extensive phylogenetic studies including *M. legis* are urged.

4.3 Function(s) of the opal layer

The calcitic shell of Foraminifera may potentially originate from the detoxification of harmful Ca^{2+} ions within the cell (Simkiss, 1977; Kaźmierczak et al., 1985), the resultant test serving various functions such as protection against predation, buoyancy control, or facilitation of reproduction. Similarly, the opal layer may also be initially secreted as a detoxification byproduct (Marron et al., 2016), with additional function(s) beneficial for the foraminifera's success in deep-sea environments. Undoubtedly, the test also acts as a protective physical barrier against unfavourable physical or chemical conditions of the environment (Marszalek et al., 1969; Wetmore, 1987), particularly considering the chemical and mechanical characteristics of opal.

The only other foraminifera with an opaline test, *M. legis*, is found in relatively deep habitats (> 4400 m depth; Burmistrova, 1978; Resig et al., 1980) below the carbonate compensation depth (CCD), where calcitic foraminifera are very rare (Resig et al., 1980; Gooday et al., 2008). This suggests that secreting an opaline test could be an adaptation to environments in which producing and maintaining a calcitic shell are challenging. However, *B. spissa* specimens in the present study were found at much shallower depths (1410 m) well above the CCD (∼ 4500–5000 m depth in the northwestern Pacific; Chen et al., 1988), in samples where other calcitic species occur abundantly and without any visible signs of dissolution. This indicates that calcification is not limiting in these environments and suggests that the opaline and calcitic parts of the test could serve different and/or complementary function(s).

Diatom frustules, made of opal, are known to possess incredible mechanical properties such as remarkable light weight, strength, and structural integrity, among other functions (Hamm et al., 2003; Knoll and Kotrc, 2015; Aitken et al., 2016). Despite not observing any microstructures in the opal layer of *B. spissa* such as in diatom frustules, it is plausible that the opal layer may serve as a supplementary mechanical support for the calcitic shell, enhancing the mechanical integrity of the entire test. However, the occurrence of other species with a more fragile test compared to *B. spissa* at the same location, such as *Chilostomella*, does not support this hypothesis. Achieving better mechanical resistance regarding compressive forces could represent an advantage in the context of protection against potential predation. This might be especially true for propagules or juveniles, since the opal layer is the thickest in old chambers at the proloculus side.

The thick opal layer in the proloculus might indicate a function associated with propagule dispersion. Compared to calcite, opal has a lower density (2.7 and 1.9–2.2 $g\,cm^{-3}$, respectively; Mukherjee, 2012), which could facilitate resuspension, movements, and/or propagation of juveniles by decreasing the density of young tests compared to a test of equivalent thickness made only of calcite. Some benthic foraminiferal species are hypothesised to have a floating propagule stage to ensure long-distance dispersal to different habitats (Alve and Goldstein, 2010). Alternatively, another *Bolivina* species, *Bolivina variabilis*, was reported to have a tychopelagic life strategy and to be able to grow and calcify in benthic and in planktic settings depending on its ontogenetic stage (Darling et al., 2009; Kucera et al., 2017). The low $\delta^{18}O$ in the proloculus part of *B. spissa* (Figs. S5 and S6) could indicate that juvenile specimens did calcify at higher temperatures compared to adult chambers, such as is the case for the congeneric *B. variabilis* (Darling et al., 2009). However, the isotopic shift between old and new chambers was not observed systematically in *B. spissa*, even among small individuals. Finally, the fact that an opal layer was not observed in decalcified *B. variabilis* (Fig. S10) does not support the hypothesis that the opal layer observed in *B. spissa* could be involved in a buoyancy function.

Opaline silica is acid-resistant and ∼ 5 times more resistant to abrasion than calcite (Mukherjee, 2012). These two parameters might be of great value regarding protection against predation (Hickman and Lipps, 1983). For instance, parasitic foraminifera were reported to drill holes into the shells of bivalves by corrosion (i.e. dissolution; Cedhagen, 1994) and into the calcitic tests of other foraminifera species (by an unknown mechanism; Hallock and Talge, 1994). Drilling by mechanical abrasion, presumably the result of predation by nematodes, was also found on foraminiferal tests belonging to *Rosalina* and *Bolivina* genera (Sliter, 1971). Additionally, selective predation on foraminifera from the Galapagos hydrothermal mounds by a naticid gastropod was reported by Arnold et al. (1985), and other unknown organisms were suggested to have bored holes into foraminiferal tests (Nielsen, 1999; Hickman and Lipps, 1983). Drilling strategies, by either chemical etching or mechanical abrasion, would be much more difficult or even inefficient against an opal layer, which would act as a protective layer preventing predators from accessing the cell content. Foraminifera in Sagami Bay are potential prey for a variety of metazoans (e.g. molluscs, copepods, or nematodes; Nomaki et al., 2008), supporting the hypothesis of protection against predation for *Bolivina* in this study. In the case of complete ingestion by another organism (deliberate or fortuitous; e.g. Herbert, 1991; Hickman and Lipps, 1983; Lipps, 1983), some foraminifera may survive relatively short passage in the gut by retracting in their test (Culver and Lipps, 2003), and the opaline silica layer may further help to avoid

complete dissolution of the test in that specific case. Environmental SEM observations performed on another *Bolivina* morphospecies sampled from a nearby site in Sagami Bay (off the coast of Misaki; 740 m depth; 35°04.30′ N, 139°32.50′ E) indicate that this species possesses structures comparable to *B. spissa* underlying the calcitic test after decalcification (Fig. S11). While these observations were only made on a few dead specimens, we occasionally observed predatory marks on their tests, with the calcitic test being totally bored but with an underlying layer incompletely pierced (Fig. S12). Although these observations were made on a different *Bolivina* morphospecies, they suggest that protection from a drilling strategy occurs at a nearby location for the same genus. However, additional studies are necessary to confirm the exact nature of the structure exposed after decalcification in this different morphospecies and the origin of these borings.

We hypothesise that a plausible function of this opal layer coating the inside part of the calcitic shell would be for protection against predators, as it is efficient against chemical or abrasive boring attacks and could potentially increase the overall strength of the test in the case of significant compressive mechanical stress. Further investigations are needed to validate this hypothesis and define possible other, potentially non-exclusive, functions.

4.4 Implication(s) for palaeoproxies and biogeochemical cycles

Compared to the aperture side of *B. spissa* where C and O isotopic compositions were close to equilibrium values, lower calcitic $\delta^{13}C$ and $\delta^{18}O$ values were principally observed at the proloculus side where the Si layer is the thickest. Moreover, the isotopic values of the proloculus side may be overwritten by the deposition of secondary calcite added during growth, lowering the $\delta^{18}O$ and $\delta^{13}C$ isotopic ratios that were measured in this study even further. This is confirmed by the fact that small specimens (i.e. with fewer chambers, younger) showed lower $\delta^{13}C$ and $\delta^{18}O$ values compared to larger specimens (i.e. with more chambers, older). These offsets can be explained by either "vital effects" during calcification or different habitat temperatures during the juvenile stage. Alternatively, the higher silicification observed on the proloculus side compared to the aperture side may possibly have altered the cytoplasmic activity and/or resource partitioning regarding C and O in the cell, explaining the differences in isotopic composition between old and new chambers. Ishimura et al. (2012) suggested that the variations in intracellular chemistry affect the isotopic composition of the calcite shell. This might result from the more intense Si precipitation on the proloculus side (thicker opal layer) compared to the apertural side of the test in *B. spissa*, assuming simultaneous calcite precipitation and opal formation within putative SDVs. However, the decreased $\delta^{18}O$ values in the proloculus part of *B. spissa* were not observed in all specimens, suggesting there could be another mechanism (or mechanisms) responsible for such light isotopic compositions. Increasing the number of specimens analysed and conducting high-spatial-resolution analyses of isotopic compositions, such as secondary ionisation mass spectrometry (SIMS) or laser ablation inductively coupled mass spectrometry (ICP-MS), will provide further insight into a potential isotopic composition shift regarding chamber position.

The test composition of calcitic Foraminifera is widely used for palaeoreconstruction and palaeoproxy purposes (e.g. Zachos et al., 2001; Katz et al., 2010), and *B. spissa* has been used in this context (Glock et al., 2012; Koho et al., 2017). Therefore, refined geochemical composition analyses of the opaline layer, not performed in our study, are necessary to assess its impact in the context of the use of *Bolivina* shells as a geochemical palaeoproxy. On the other hand, the presence of this opaline layer may open a whole new opportunity to develop novel proxies based on the glassy part of the *B. spissa* test, especially in oxygen-depleted environments. Such proxies exist, for instance for diatoms, silicifying sponges, or radiolarians, for which the isotopic composition may be used to trace dissolved silica concentration, pH, or nitrate utilisation through geological times (e.g. De La Rocha, 2006; Hendry et al., 2010; Donald et al., 2020; Trower et al., 2021).

Bolivina spissa is a cosmopolitan shallow infaunal species regularly reported at several different locations in the northeastern Pacific such as the Santa Monica Basin, Monterey Bay cold seeps, or the Cascadia convergent margin (e.g. Cushman, 1926; Bernhard et al., 2001; Heinz et al., 2005; Keating-Bitonti and Payne, 2017) as well as in the southeastern Pacific at the Peruvian margin (Glock et al., 2011). The species is also found in the northwestern Pacific around Japan (Kitazato et al., 2000; Nomaki et al., 2006; Glud et al., 2009; Fontanier et al., 2014; Koho et al., 2017) and in the Sea of Okhotsk (Bubenshchikova et al., 2008). The wide geographic distribution and abundance of *B. spissa* emphasise its potential to be a good palaeoproxy using its opaline test. Foraminifera are known to be major protagonists contributing to the organic and inorganic carbon cycle (for organic matter degradation, see, for example, Gooday et al., 1992, and Moodley et al., 2000; for carbonate production, see, for example, Langer, 2008) and nitrogen cycle (for denitrifying species such as *B. spissa*; e.g. Pina-Ochoa et al., 2010; Xu et al., 2017; Glock et al., 2019; Woehle et al., 2022). Furthermore, prior TEM observations of *Bolivina pacifica* (Fig. 4 in Bernhard et al., 2010) and *Bolivina argentea* (Fig. 1a in Bernhard et al., 2012) have revealed similar structures to those observed in *B. spissa* in this study, suggesting the potential presence of an opal layer beneath the calcitic test of other *Bolivina* species. If silicification were ultimately found to be more widespread than previously known, either among the genus *Bolivina* or possibly among other Foraminifera genera, this group could also participate in Si cycling, adding

to the already significant role of other Rhizaria in this cycle (Llopis Monferrer et al., 2020).

5 Conclusions

We report that the foraminifera *Bolivina spissa* exhibits a composite test made of an opal layer coating the internal part of the calcitic test. The thickness pattern of the opal layer, thick in the proloculus and thinning toward newer chambers, coupled to the identification of organelles involved in silica precipitation found for the first time in Foraminifera, ascribed to silica deposition vesicles (SDVs), indicates that the *B. spissa* can silicify by itself. The deposition of opal appears to be discontinuous and to take place after calcite precipitation, occurring in different chambers at the same time. We propose that the opal layer may serve as a protective barrier against predators able to drill holes chemically or mechanically in the calcitic tests of Foraminifera. However, other (non-exclusive) functions could exist and need to be investigated further. The presence of this opal layer below the calcitic test of the cosmopolitan *B. spissa*, which had until now been overlooked, raises questions about the extent of silicification in Foraminifera. The only other known silicifying species branches relatively far on phylogenetic trees and belongs to another foraminiferal class. At the same time, preliminary observations of another *Bolivina* morphospecies exhibiting analogous structures below calcite could indicate that this trait may be more widespread than previously assumed. While the presence of this opal layer below the calcitic test may influence palaeoceanographic reconstruction using test composition, it may also lead to the development of a new palaeoproxy (or palaeoproxies) based on this layer.

Data availability. Raw data are available in the Supplement attached to this paper.

Supplement. The supplement related to this article is available online at: https://doi.org/10.5194/bg-21-3271-2024-supplement.

Author contributions. JR: conceptualisation, sampling, environmental SEM sample preparation and data acquisition, data interpretation, original draft writing. SO: sampling, cryo-SEM and FTIR sample preparation and data acquisition, data interpretation. YI: sampling, data interpretation. KU: TEM sample preparation and data acquisition. AT: TEM sample preparation. KO: foraminifera picking, sample preparation. NI: FTIR data acquisition, data interpretation. TI: isotopic data acquisition and interpretation. MT: data interpretation. HN: conceptualisation, sampling, data interpretation. All co-authors participated in the writing, review, and editing process.

Competing interests. The contact author has declared that none of the authors has any competing interests.

Disclaimer. Publisher's note: Copernicus Publications remains neutral with regard to jurisdictional claims made in the text, published maps, institutional affiliations, or any other geographical representation in this paper. While Copernicus Publications makes every effort to include appropriate place names, the final responsibility lies with the authors.

Acknowledgements. We are grateful to the captains, crew members, and onboard scientists of R/V *Yokosuka* as well as the operation team of HOV *Shinkai 6500* for their help during samples collection. We would like to thank Takazo Shibuya (JAMSTEC) for his help regarding FTIR measurements and Elena Golikova for generously providing us with literature that would have otherwise been difficult to access. This paper benefited from the valuable contributions of Lennart de Nooijer and the anonymous reviewer during the reviewing process.

Financial support. This research has been supported by the Japan Society for the Promotion of Science (grant nos. P21729 and 21H01202).

Review statement. This paper was edited by Jack Middelburg and reviewed by Lennart de Nooijer and one anonymous referee.

References

Aitken, Z. H., Luo, S., Reynolds, S. N., Thaulow, C., and Greer, J. R.: Microstructure provides insights into evolutionary design and resilience of *Coscinodiscus* sp. frustule, P. Natl. Acad. Sci. USA, 113, 2017–2022, https://doi.org/10.1073/pnas.1519790113, 2016.

Alve, E. and Goldstein, S. T.: Dispersal, survival and delayed growth of benthic foraminiferal propagules, J. Sea Res., 63, 36–51, https://doi.org/10.1016/j.seares.2009.09.003, 2010.

Anderson, O. R.: Cytoplasmic origin and surface deposition of siliceous structures in Sarcodina, Protoplasma, 181, 61–77, https://doi.org/10.1007/BF01666389, 1994.

Arnold, A. J., d'Escrivan, F., and Parker, W. C.: Predation and avoidance responses in the foraminifera of the Galapagos hydrothermal mounds, J. Foramin. Res., 15, 38–42, https://doi.org/10.2113/gsjfr.15.1.38, 1985.

Bé, A. W. H. and Lott, L.: Shell Growth and Structure of Planktonic Foraminifera, Science, 145, 823–824, https://doi.org/10.1126/science.145.3634.823, 1964.

Bernhard, J. M., Buck, K. R., and Barry, J. P.: Monterey Bay cold-seep biota: Assemblages, abundance, and ultrastructure of living foraminifera, Deep-Sea Res. Pt. I, 48, 2233–2249, https://doi.org/10.1016/S0967-0637(01)00017-6, 2001.

Bernhard, J. M., Goldstein, S. T., and Bowser, S. S.: An ectobiont-bearing foraminiferan, *Bolivina pacifica*, that

inhabits microxic pore waters: cell-biological and paleoceanographic insights, Environ. Microbiol., 12, 2107–2119, https://doi.org/10.1111/j.1462-2920.2009.02073.x, 2010.

Bernhard, J. M., Casciotti, K. L., McIlvin, M. R., Beaudoin, D. J., Visscher, P. T., and Edgcomb, V. P.: Potential importance of physiologically diverse benthic foraminifera in sedimentary nitrate storage and respiration, Journal of Geophysical Research: Biogeosciences, 117, https://doi.org/10.1029/2012JG001949, 2012.

Borrelli, C., Panieri, G., Dahl, T. M., and Neufeld, K.: Novel biomineralization strategy in calcareous foraminifera, Sci. Rep.-UK, 8, 10201, https://doi.org/10.1038/s41598-018-28400-2, 2018.

Brady, H. B.: Report on the Foraminifera dredged by H.M.S. Challenger during the Years 1873–1876, Report on the Scientific Results of the Voyage of H.M.S. Challenger during the years 1873–76, Zoology, 9, 1–814, https://doi.org/10.5962/bhl.title.6513, 1884.

Brümmer, F.: Living Inside a Glass Box – Silica in Diatoms, in: Silicon Biomineralization: Biology – Biochemistry – Molecular Biology – Biotechnology, edited by: Müller, W. E. G., Springer, Berlin, Heidelberg, 3–10, https://doi.org/10.1007/978-3-642-55486-5_1, 2003.

Bubenshchikova, N., Nürnberg, D., Lembke-Jene, L., and Pavlova, G.: Living benthic foraminifera of the Okhotsk Sea: Faunal composition, standing stocks and microhabitats, Mar. Micropaleontol., 69, 314–333, https://doi.org/10.1016/j.marmicro.2008.09.002, 2008.

Burki, F., Roger, A. J., Brown, M. W., and Simpson, A. G. B.: The New Tree of Eukaryotes, Trends Ecol. Evol., 35, 43–55, https://doi.org/10.1016/j.tree.2019.08.008, 2020.

Burmistrova, I. I.: K stratigrafii glubokovodnykh osadkov vostochnoy chasti Indiyskogo Okeana po bentosnym foraminiferam [On the stratigraphy of deep sea deposits in the eastern part of the Indian Ocean, based on benthic foraminifera], in: Morskaya Mikropaleontologiya, Okeanograficheskaya Komissiya, Akademiya Nauk SSSR, Moscow,163–170, 1978.

Cedhagen, T.: Taxonomy and biology of *Hyrrokkin sarcophaga* gen. et sp. n., a parasitic foraminiferan (Rosalinidae), Sarsia, 79, 65–82, https://doi.org/10.1080/00364827.1994.10413549, 1994.

Cesbron, F., Geslin, E., Jorissen, F. J., Delgard, M. L., Charrieau, L., Deflandre, B., Jézéquel, D., Anschutz, P., and Metzger, E.: Vertical distribution and respiration rates of benthic foraminifera: Contribution to aerobic remineralization in intertidal mudflats covered by *Zostera noltei* meadows, Estuar. Coast. Shelf S., 179, 23–38, https://doi.org/10.1016/j.ecss.2015.12.005, 2016.

Chen, C. T. A., Feely, R. A., and Gendron, J. F.: Lysocline, Calcium Carbonate Compensation Depth, and Calcareous Sediments in the North Pacific Ocean, Pac. Sci., 42, 237–252, 1988.

Culver, S. J.: Early Cambrian Foraminifera from West Africa, Science, 254, 689–691, https://doi.org/10.1126/science.254.5032.689, 1991.

Culver, S. J. and Lipps, J. H.: Predation on and by Foraminifera, in: Predator—Prey Interactions in the Fossil Record, edited by: Kelley, P. H., Kowalewski, M., and Hansen, T. A., Springer US, Boston, MA, 7–32, https://doi.org/10.1007/978-1-4615-0161-9_2, 2003.

Cushman, J. A.: Some Pliocene *Bolivinas* from California, Contributions from the Cushman laboratory for foraminiferal research, 2, 40–47, 1926.

Darling, K. F., Thomas, E., Kasemann, S. A., Seears, H. A., Smart, C. W., and Wade, C. M.: Surviving mass extinction by bridging the benthic/planktic divide, P. Natl. Acad. Sci. USA, 106, 12629–12633, https://doi.org/10.1073/pnas.0902827106, 2009.

De La Rocha, C. L.: Opal-based isotopic proxies of paleoenvironmental conditions, Global Biogeochem. Cy., 20, GB4S09, https://doi.org/10.1029/2005GB002664, 2006.

de Nooijer, L. J., Spero, H. J., Erez, J., Bijma, J., and Reichart, G. J.: Biomineralization in perforate foraminifera, Earth-Science Reviews, 135, 48–58, https://doi.org/10.1016/j.earscirev.2014.03.013, 2014.

de Nooijer, L. J., Pacho Sampedro, L., Jorissen, F. J., Pawlowski, J., Rosenthal, Y., Dissard, D., and Reichart, G. J.: 500 million years of foraminiferal calcification, Earth-Sci. Rev., 243, 104484, https://doi.org/10.1016/j.earscirev.2023.104484, 2023.

De Stefano, L., De Stefano, M., Rea, I., Moretti, L., Bismuto, A., Maddalena, P., and Rendina, I.: Optical characterisation of biological nano-porous silica structures, Proc. SPIE, 59250S, https://doi.org/10.1117/12.619450, 2005.

Donald, H. K., Foster, G. L., Fröhberg, N., Swann, G. E. A., Poulton, A. J., Moore, C. M., and Humphreys, M. P.: The pH dependency of the boron isotopic composition of diatom opal (*Thalassiosira weissflogii*), Biogeosciences, 17, 2825–2837, https://doi.org/10.5194/bg-17-2825-2020, 2020.

Drum, R. W. and Pankratz, H. S.: Post mitotic fine structure of *Gomphonema parvulum*, J. Ultra Mol. Struct. R., 10, 217–223, https://doi.org/10.1016/s0022-5320(64)80006-x, 1964.

Dubicka, Z.: Chamber arrangement versus wall structure in the high-rank phylogenetic classification of Foraminifera, Acta Palaeontologica Polonica, 64, 1–18, https://doi.org/10.4202/app.00564.2018, 2019.

Echols, R. J.: Distribution of Foraminifera in Sediments of the Scotia Sea Area, Antarctic Waters, in: Antarctic Oceanology I, American Geophysical Union (AGU), 93–168, 1971.

Ehrlich, H. L., Newman, D. K., and Kappler, A. (Eds.): Ehrlich's Geomicrobiology, 6th edn., CRC Press, 656 pp., https://doi.org/10.1201/b19121, 2016.

Foissner, W., WEissenbacher, B., Krautgartner, W.-D., and Lütz-Meindl, U.: A Cover of Glass: First Report of Biomineralized Silicon in a Ciliate, *Maryna umbrellata* (Ciliophora: Colpodea), J. Eukaryot. Microbiol., 56, 519–530, https://doi.org/10.1111/j.1550-7408.2009.00431.x, 2009.

Fontanier, C., Duros, P., Toyofuku, T., Oguri, K., Koho, K. A., Buscail, R., Gremare, A., Radakovitch, O., Deflandre, B., de Nooijer, L. J., Bichon, S., Goubet, S., Ivanovsky, A., Chabaud, G., Menniti, C., Reichart, G.-J., and Kitazato, H.: LIVING (STAINED) DEEP-SEA FORAMINIFERA OFF HACHINOHE (NE JAPAN, WESTERN PACIFIC): ENVIRONMENTAL INTERPLAY IN OXYGEN-DEPLETED ECOSYSTEMS, J. Foramin. Res., 44, 281–299, https://doi.org/10.2113/gsjfr.44.3.281, 2014.

Garrone, R., Simpson, T. L., and Pottu-Boumendil, J.: Ultrastructure and Deposition of Silica in Sponges, in: Silicon and Siliceous Structures in Biological Systems, edited by: Simpson, T. L. and Volcani, B. E., Springer, New York, NY, https://doi.org/10.1007/978-1-4612-5944-2_17, 495–525, 1981.

Glock, N., Eisenhauer, A., Milker, Y., Liebetrau, V., Schönfeld, J., Mallon, J., Sommer, S., and Hensen, C.: Environmental Influences on the Pore Density of *Boliv-*

ina Spissa (Cushman), J. Foramin. Res., 41, 22–32, https://doi.org/10.2113/gsjfr.41.1.22, 2011.

Glock, N., Eisenhauer, A., Liebetrau, V., Wiedenbeck, M., Hensen, C., and Nehrke, G.: EMP and SIMS studies on Mn/Ca and Fe/Ca systematics in benthic foraminifera from the Peruvian OMZ: a contribution to the identification of potential redox proxies and the impact of cleaning protocols, Biogeosciences, 9, 341–359, https://doi.org/10.5194/bg-9-341-2012, 2012.

Glock, N., Roy, A.-S., Romero, D., Wein, T., Weissenbach, J., Revsbech, N. P., Høgslund, S., Clemens, D., Sommer, S., and Dagan, T.: Metabolic preference of nitrate over oxygen as an electron acceptor in foraminifera from the Peruvian oxygen minimum zone, P. Natl. Acad. Sci. USA, 116, 2860–2865, https://doi.org/10.1073/pnas.1813887116, 2019.

Glud, R. N., Thamdrup, B., Stahl, H., Wenzhoefer, F., Glud, A., Nomaki, H., Oguri, K., Revsbech, N. P., and Kitazato, H.: Nitrogen cycling in a deep ocean margin sediment (Sagami Bay, Japan), Limnol. Oceanogr., 54, 723–734, https://doi.org/10.4319/lo.2009.54.3.0723, 2009.

Goldstein, S. T. and Corliss, B. H.: Deposit feeding in selected deep-sea and shallow-water benthic foraminifera, Deep-Sea Res. Pt. I, 41, 229–241, https://doi.org/10.1016/0967-0637(94)90001-9, 1994.

Gooday, A. J., Levin, L. A., Linke, P., and Heeger, T.: The Role of Benthic Foraminifera in Deep-Sea Food Webs and Carbon Cycling, in: Deep-Sea Food Chains and the Global Carbon Cycle, edited by: Rowe, G. T. and Pariente, V., Springer Netherlands, Dordrecht, https://doi.org/10.1007/978-94-011-2452-2_5, 63–91, 1992.

Gooday, A. J., Nomaki, H., and Kitazato, H.: Modern deep-sea benthic foraminifera: a brief review of their morphology-based biodiversity and trophic diversity, Geological Society, London, Special Publications, 303, 97–119, https://doi.org/10.1144/SP303.8, 2008.

Greenwood, N. N. and Earnshaw, A.: Chemistry of the Elements, Elsevier, 1365 pp., https://doi.org/10.1016/C2009-0-30414-6, 1997.

Groussin, M., Pawlowski, J., and Yang, Z.: Bayesian relaxed clock estimation of divergence times in foraminifera, Mol. Phylogenet. Evol., 61, 157–166, https://doi.org/10.1016/j.ympev.2011.06.008, 2011.

Gupta, B. K. S.: Modern Foraminifera, Springer Science & Business Media, 368 pp., https://doi.org/10.1007/0-306-48104-9, 2003.

Hallock, P. and Talge, H.: A Predatory Foraminifer, *Floresina amphiphaga*, n. sp., from the Florida Keys, J. Foramin. Res., 24, 210–213, https://doi.org/10.2113/gsjfr.24.4.210, 1994.

Hamm, C. E., Merkel, R., Springer, O., Jurkojc, P., Maier, C., Prechtel, K., and Smetacek, V.: Architecture and material properties of diatom shells provide effective mechanical protection, Nature, 421, 841–843, https://doi.org/10.1038/nature01416, 2003.

Hansen, H. J.: Shell construction in modern calcareous Foraminifera, in: Modern Foraminifera, edited by: Sen Gupta, B. K., Springer Netherlands, Dordrecht, https://doi.org/10.1007/0-306-48104-9_4, 57–70, 2003.

Heinz, P., Sommer, S., Pfannkuche, O., and Hemleben, C.: Living benthic foraminifera in sediments influenced by gas hydrates at the Cascadia convergent margin, NE Pacific, Mar. Ecol. Prog. Ser., 304, 77–89, https://doi.org/10.3354/meps304077, 2005.

Hendry, K. R., Georg, R. B., Rickaby, R. E. M., Robinson, L. F., and Halliday, A. N.: Deep ocean nutrients during the Last Glacial Maximum deduced from sponge silicon isotopic compositions, Earth Planet. Sc. Lett., 292, 290–300, https://doi.org/10.1016/j.epsl.2010.02.005, 2010.

Hendry, K. R., Marron, A. O., Vincent, F., Conley, D. J., Gehlen, M., Ibarbalz, F. M., Quéguiner, B., and Bowler, C.: Competition between Silicifiers and Non-silicifiers in the Past and Present Ocean and Its Evolutionary Impacts, Frontiers in Marine Science, 5, 22, https://doi.org/10.3389/fmars.2018.00022, 2018.

Herbert, D. G.: Foraminiferivory in a *Puncturella* (Gastropoda: Fissurellidae), J. Mollus. Stud., 57, 127–129, https://doi.org/10.1093/mollus/57.1.127, 1991.

Hickman, C. S. and Lipps, J. H.: Foraminiferivory; selective ingestion of foraminifera and test alterations produced by the neogastropod *Olivella*, J. Foramin. Res., 13, 108–114, https://doi.org/10.2113/gsjfr.13.2.108, 1983.

Holzmann, M. and Pawlowski, J.: An updated classification of rotaliid foraminifera based on ribosomal DNA phylogeny, Mar. Micropaleontol., 132, 18–34, https://doi.org/10.1016/j.marmicro.2017.04.002, 2017.

Ishimura, T., Tsunogai, U., and Gamo, T.: Stable carbon and oxygen isotopic determination of sub-microgram quantities of $CaCO_3$ to analyze individual foraminiferal shells, Rapid Commun. Mass Sp., 18, 2883–2888, https://doi.org/10.1002/rcm.1701, 2004.

Ishimura, T., Tsunogai, U., and Nakagawa, F.: Grain-scale heterogeneities in the stable carbon and oxygen isotopic compositions of the international standard calcite materials (NBS 19, NBS 18, IAEA-CO-1, and IAEA-CO-8), Rapid Commun. Mass Sp., 22, 1925–1932, https://doi.org/10.1002/rcm.3571, 2008.

Ishimura, T., Tsunogai, U., Hasegawa, S., Nakagawa, F., Oi, T., Kitazato, H., Suga, H., and Toyofuku, T.: Variation in stable carbon and oxygen isotopes of individual benthic foraminifera: tracers for quantifying the magnitude of isotopic disequilibrium, Biogeosciences, 9, 4353–4367, https://doi.org/10.5194/bg-9-4353-2012, 2012.

Jauffrais, T., LeKieffre, C., Koho, K. A., Tsuchiya, M., Schweizer, M., Bernhard, J. M., Meibom, A., and Geslin, E.: Ultrastructure and distribution of kleptoplasts in benthic foraminifera from shallow-water (photic) habitats, Mar. Micropaleontol., 138, 46–62, https://doi.org/10.1016/j.marmicro.2017.10.003, 2018.

Jones, R. W.: Foraminifera and their Applications, Cambridge University Press, 407 pp., ISBN 978-1-107-03640-6, 2013.

Katz, M. E., Cramer, B. S., Franzese, A., Hönisch, B., Miller, K. G., Rosenthal, Y., and Wright, J. D.: Traditional and emerging geochemical proxies in foraminifera, J. Foramin. Res., 40, 165–192, https://doi.org/10.2113/gsjfr.40.2.165, 2010.

Kaźmierczak, J., Ittekkot, V., and Degens, E. T.: Biocalcification through time: environmental challenge and cellular response, Palaeont. Z., 59, 15–33, https://doi.org/10.1007/BF02985996, 1985.

Keating-Bitonti, C. R. and Payne, J. L.: Ecophenotypic responses of benthic foraminifera to oxygen availability along an oxygen gradient in the California Borderland, Mar. Ecol., 38, e12430, https://doi.org/10.1111/maec.12430, 2017.

Kitazato, H., Shirayama, Y., Nakatsuka, T., Fujiwara, S., Shimanaga, M., Kato, Y., Okada, Y., Kanda, J., Yamaoka, A., Masuzawa, T., and Suzuki, K.: Seasonal phytodetritus deposition and responses of bathyal benthic foraminiferal pop-

ulations in Sagami Bay, Japan: preliminary results from "Project Sagami 1996–1999," Mar. Micropaleontol., 40, 135–149, https://doi.org/10.1016/S0377-8398(00)00036-0, 2000.

Knoll, A. H. and Kotrc, B.: Protistan Skeletons: A Geologic History of Evolution and Constraint, in: Evolution of Lightweight Structures: Analyses and Technical Applications, edited by: Hamm, C., Springer Netherlands, Dordrecht, https://doi.org/10.1007/978-94-017-9398-8_1, 1–16, 2015.

Koho, K. A., de Nooijer, L. J., Fontanier, C., Toyofuku, T., Oguri, K., Kitazato, H., and Reichart, G.-J.: Benthic foraminiferal Mn/Ca ratios reflect microhabitat preferences, Biogeosciences, 14, 3067–3082, https://doi.org/10.5194/bg-14-3067-2017, 2017.

Krabberød, A. K., Orr, R. J. S., Bråte, J., Kristensen, T., Bjørklund, K. R., and Shalchian-Tabrizi, K.: Single Cell Transcriptomics, Mega-Phylogeny, and the Genetic Basis of Morphological Innovations in Rhizaria, Mol. Biol. Evol., 34, 1557–1573, https://doi.org/10.1093/molbev/msx075, 2017.

Kucera, M., Silye, L., Weiner, A. K. M., Darling, K., Lübben, B., Holzmann, M., Pawlowski, J., Schönfeld, J., and Morard, R.: Caught in the act: anatomy of an ongoing benthic–planktonic transition in a marine protist, J. Plankton Res., 39, 436–449, https://doi.org/10.1093/plankt/fbx018, 2017.

Langer, M. R.: Assessing the Contribution of Foraminiferan Protists to Global Ocean Carbonate Production1, J. Eukaryot. Microbiol., 55, 163–169, https://doi.org/10.1111/j.1550-7408.2008.00321.x, 2008.

Larkin, P.: Infrared and Raman Spectroscopy: Principles and Spectral Interpretation, Elsevier, 239 pp., https://doi.org/10.1016/C2015-0-00806-1, 2011.

LeKieffre, C., Bernhard, J. M., Mabilleau, G., Filipsson, H. L., Meibom, A., and Geslin, E.: An overview of cellular ultrastructure in benthic foraminifera: New observations of rotalid species in the context of existing literature, Mar. Micropaleontol., 138, 12–32, https://doi.org/10.1016/j.marmicro.2017.10.005, 2018.

Lipps, J. H.: Test Structure in Foraminifera, Annu. Rev. Microbiol., 27, 471–486, https://doi.org/10.1146/annurev.mi.27.100173.002351, 1973.

Lipps, J. H.: Biotic Interactions in Benthic Foraminifera, in: Biotic Interactions in Recent and Fossil Benthic Communities, edited by: Tevesz, M. J. S. and McCall, P. L., Springer US, Boston, MA, 331–376, https://doi.org/10.1007/978-1-4757-0740-3_8, 1983.

Llopis Monferrer, N., Boltovskoy, D., Tréguer, P., Sandin, M. M., Not, F., and Leynaert, A.: Estimating Biogenic Silica Production of Rhizaria in the Global Ocean, Global Biogeochem. Cy., 34, e2019GB006286, https://doi.org/10.1029/2019GB006286, 2020.

Lowenstam, H. A.: Opal Precipitation by Marine Gastropods (Mollusca), Science, 171, 487–490, https://doi.org/10.1126/science.171.3970.487, 1971.

Marron, A. O., Ratcliffe, S., Wheeler, G. L., Goldstein, R. E., King, N., Not, F., de Vargas, C., and Richter, D. J.: The Evolution of Silicon Transport in Eukaryotes, Mol. Biol. Evol., 33, 3226–3248, https://doi.org/10.1093/molbev/msw209, 2016.

Marszalek, D. S., Wright, R. C., and Hay, W. W.: Function of the Test in Foraminifera, Gulf Coast. Assoc. Geological Societies Trans., 19, 341–352, 1969.

Mayerhöfer, T. G., Pahlow, S., Hübner, U., and Popp, J.: CaF_2: An Ideal Substrate Material for Infrared Spectroscopy?, Anal. Chem., 92, 9024–9031, https://doi.org/10.1021/acs.analchem.0c01158, 2020.

Moodley, L., Boschker, H. T. S., Middelburg, J. J., Pel, R., Herman, P. M. J., de Deckere, E., and Heip, C. H. R.: Ecological significance of benthic foraminifera: ^{13}C labelling experiments, Mar. Ecol. Prog. Ser., 202, 289–295, https://doi.org/10.3354/meps202289, 2000.

Mukherjee, S.: Applied Mineralogy: Applications in Industry and Environment, Springer Science & Business Media, 585 pp., https://doi.org/10.1007/978-94-007-1162-4, 2012.

Murray, J. W.: Ecology and Applications of Benthic Foraminifera, Cambridge University Press, Cambridge, https://doi.org/10.1017/CBO9780511535529, 2006.

Murray, J. W.: Biodiversity of living benthic foraminifera: How many species are there?, Mar. Micropaleontol., 64, 163–176, https://doi.org/10.1016/j.marmicro.2007.04.002, 2007.

Nagai, Y., Uematsu, K., Chen, C., Wani, R., Tyszka, J., and Toyofuku, T.: Weaving of biomineralization framework in rotaliid foraminifera: implications for paleoceanographic proxies, Biogeosciences, 15, 6773–6789, https://doi.org/10.5194/bg-15-6773-2018, 2018.

Nardelli, M. P., Barras, C., Metzger, E., Mouret, A., Filipsson, H. L., Jorissen, F., and Geslin, E.: Experimental evidence for foraminiferal calcification under anoxia, Biogeosciences, 11, 4029–4038, https://doi.org/10.5194/bg-11-4029-2014, 2014.

Nielsen, K. S. S.: Foraminiferivory revisited: a preliminary investigation of holes in foraminifera, B. Geol. Soc. Denmark, 45, 139–142, 1999.

Nomaki, H., Heinz, P., Nakatsuka, T., Shimanaga, M., Ohkouchi, N., Ogawa, N. O., Kogure, K., Ikemoto, E., and Kitazato, H.: Different ingestion patterns of 13C-labeled bacteria and algae by deep-sea benthic foraminifera, Mar. Ecol. Prog. Ser., 310, 95–108, https://doi.org/10.3354/meps310095, 2006.

Nomaki, H., Ogawa, N. O., Ohkouchi, N., Suga, H., Toyofuku, T., Shimanaga, M., Nakatsuka, T., and Kitazato, H.: Benthic foraminifera as trophic links between phytodetritus and benthic metazoans: carbon and nitrogen isotopic evidence, Mar. Ecol. Prog. Ser., 357, 153–164, https://doi.org/10.3354/meps07309, 2008.

Okada, S., Richirt, J., Tame, A., and Nomaki, H.: Rapid Freezing and Cryo-SEM-EDS Imaging of Foraminifera (Unicellular Eukaryotes) Using a Conductive Viscous Cryogenic Glue, Microsc. Microanal., 30, 359–367, https://doi.org/10.1093/mam/ozae026, 2024.

Orsi, W. D., Morard, R., Vuillemin, A., Eitel, M., Wörheide, G., Milucka, J., and Kucera, M.: Anaerobic metabolism of Foraminifera thriving below the seafloor, ISME J., 14, 2580–2594, https://doi.org/10.1038/s41396-020-0708-1, 2020.

Parker, J. H.: Ultrastructure of the Test Wall in Modern Porcelaneous Foraminifera: Implications For the Classification of the Miliolida, J. Foramin. Res., 47, 136–174, https://doi.org/10.2113/gsjfr.47.2.136, 2017.

Pawlowski, J., Holzmann, M., and Tyszka, J.: New supraordinal classification of Foraminifera: Molecules meet morphology, Mar. Micropaleontol., 100, 1–10, https://doi.org/10.1016/j.marmicro.2013.04.002, 2013.

Piña-Ochoa, E., Høgslund, S., Geslin, E., Cedhagen, T., Revsbech, N. P., Nielsen, L. P., Schweizer, M., Jorissen, F., Rysgaard, S., and Risgaard-Petersen, N.: Widespread occur-

rence of nitrate storage and denitrification among Foraminifera and Gromiida, P. Natl. Acad. Sci. USA, 107, 1148–1153, https://doi.org/10.1073/pnas.0908440107, 2010.

Reka, A. A., Pavlovski, B., Fazlija, E., Berisha, A., Pacarizi, M., Daghmehchi, M., Sacalis, C., Jovanovski, G., Makreski, P., and Oral, A.: Diatomaceous Earth: Characterization, thermal modification, and application, Open Chem., 19, 451–461, https://doi.org/10.1515/chem-2020-0049, 2021.

Resig, J. M., Lowenstam, H. A., Echols, R. J., and Weiner, S.: An extant opaline foraminifer: test ultrastructure, mineralogy, and taxonomy, in: Studies in Marine Micropaleontology and Paleoecology: A Memorial Volume to Orville L. Bandy, vol. 19, edited by: Sliter, W. V., Cushman Foundation for Foraminiferal Research, 205–214, ISBN 9781970168129, 1980.

Schindelin, J., Arganda-Carreras, I., Frise, E., Kaynig, V., Longair, M., Pietzsch, T., Preibisch, S., Rueden, C., Saalfeld, S., Schmid, B., Tinevez, J.-Y., White, D. J., Hartenstein, V., Eliceiri, K., Tomancak, P., and Cardona, A.: Fiji: an open-source platform for biological-image analysis, Nat. Methods, 9, 676–682, https://doi.org/10.1038/nmeth.2019, 2012.

Sierra, R., Mauffrey, F., Cruz, J., Holzmann, M., Gooday, A. J., Maurer-Alcalá, X., Thakur, R., Greco, M., Weiner, A. K. M., Katz, L. A., and Pawlowski, J.: Taxon-rich transcriptomics supports higher-level phylogeny and major evolutionary trends in Foraminifera, Mol. Phylogenet. Evol., 174, 107546, https://doi.org/10.1016/j.ympev.2022.107546, 2022.

Simkiss, K.: Biomineralization and detoxification, Calc. Tis. Res., 24, 199–200, https://doi.org/10.1007/BF02223316, 1977.

Sliter, W. V.: Predation on benthic foraminifers, J. Foramin. Res., 1, 20–28, https://doi.org/10.2113/gsjfr.1.1.20, 1971.

Socrates, G.: Infrared and Raman Characteristic Group Frequencies: Tables and Charts, John Wiley & Sons, 386 pp., https://doi.org/10.1021/ja0153520, 2004.

Toyofuku, T., Matsuo, M. Y., de Nooijer, L. J., Nagai, Y., Kawada, S., Fujita, K., Reichart, G.-J., Nomaki, H., Tsuchiya, M., Sakaguchi, H., and Kitazato, H.: Proton pumping accompanies calcification in foraminifera, Nat. Commun., 8, 14145, https://doi.org/10.1038/ncomms14145, 2017.

Trower, E. J., Strauss, J. V., Sperling, E. A., and Fischer, W. W.: Isotopic analyses of Ordovician–Silurian siliceous skeletons indicate silica-depleted Paleozoic oceans, Geobiology, 19, 460–472, https://doi.org/10.1111/gbi.12449, 2021.

Ujiié, Y., Ishitani, Y., Nagai, Y., Takaki, Y., Toyofuku, T., and Ishii, S.: Unique evolution of foraminiferal calcification to survive global changes, Science Advances, 9, eadd3584, https://doi.org/10.1126/sciadv.add3584, 2023.

Wetmore, K. L.: Correlations between test strength, morphology and habitat in some benthic foraminifera from the coast of Washington, J. Foramin. Res., 17, 1–13, https://doi.org/10.2113/gsjfr.17.1.1, 1987.

Woehle, C., Roy, A.-S., Glock, N., Michels, J., Wein, T., Weissenbach, J., Romero, D., Hiebenthal, C., Gorb, S. N., Schönfeld, J., and Dagan, T.: Denitrification in foraminifera has an ancient origin and is complemented by associated bacteria, P. Natl. Acad. Sci. USA, 119, e2200198119, https://doi.org/10.1073/pnas.2200198119, 2022.

Xu, Z., Liu, S., Xiang, R., and Song, G.: Live benthic foraminifera in the Yellow Sea and the East China Sea: vertical distribution, nitrate storage, and potential denitrification, Mar. Ecol. Prog. Ser., 571, 65–81, https://doi.org/10.3354/meps12135, 2017.

Zachos, J., Pagani, M., Sloan, L., Thomas, E., and Billups, K.: Trends, Rhythms, and Aberrations in Global Climate 65 Ma to Present, Science, 292, 686–693, https://doi.org/10.1126/science.1059412, 2001.